Dendritic flux instabilities in $YBa_2Cu_3O_{7-x}$ films: Effects of temperature and magnetic field ramp rate

E. Baruch-El,[1] M. Baziljevich,[1,2] B. Ya. Shapiro,[1] T. H. Johansen,[2] A. Shaulov,[1] and Y. Yeshurun[1]

[1]*Institute of Superconductivity and Institute of Nanotechnology, Department of Physics, Bar-Ilan University, Ramat-Gan, Israel*

[2]*Department of Physics, University of Oslo, 0316 Oslo, Norway*

(Received 18 May 2016; revised manuscript received 27 July 2016; published 10 August 2016)

Our recent success in triggering dendritic flux instabilities in $YBa_2Cu_3O_{7-\delta}$ (YBCO) films by applying magnetic fields at ultrahigh rates is followed here by a detailed study of the effect as a function of the field ramp rate, $\dot{B}_a$, and temperature, T. We trace the borderline in the $\dot{B}_a$-T plane separating regions of smooth, gradual flux penetration and dendritic flux avalanches. In addition, we describe the changes in the dendritic morphology in the instability region as a result of changes in either $\dot{B}_a$ or T. Our experimental results, showing a monotonic increase of the avalanche threshold field ramp rate with temperature, are discussed in the framework of existing theories. On the basis of these theories we also explain the high stability of YBCO to dendritic avalanches as compared to, e.g., MgB_2, identifying the flux flow resistivity, rather than any of the thermal parameters, as the main parameter governing the film stability.

DOI: 10.1103/PhysRevB.94.054509

I. INTRODUCTION

Under certain conditions, magnetic flux penetration into type-II superconductors may result in nonequilibrium pattern formation, such as magnetic macroturbulence [1,2], kinetic front roughening [3,4], magnetic microavalanches [5,6], and dendritic flux patterns [7]. Dendritic flux structures have been observed by magneto-optical (MO) imaging in a number of conventional superconducting films such as Nb [8–10], NbN [11–13], Nb_3Sn [14], Pb [15], a-MoSi [16], and MgB_2 [17–23]. The phenomenon reflects a thermomagnetic breakdown of the superconductor, occurring when a fluctuation weakens the pinning of some vortices, causing them to move and locally heat the material, thus reducing the pinning even further, promoting motion of more vortices. Such a runaway scenario is expected in all type-II superconductors and yet, films of high-temperature superconductors (HTSs) exposed to magnetic fields did not exhibit dendritic flux patterns, even at high fields. In an effort to generate dendritic instability in a HTS material, Leiderer *et al.* [24–26] exploited a laser to locally heat $YBa_2Cu_3O_{7-\delta}$ (YBCO) films to above the superconducting critical temperature T_c, triggering dendritic avalanches from the heated area. Nevertheless, despite numerous efforts by many researchers, a thermomagnetic instability was not observed in YBCO films in experiments similar to those generating dendritic patterns in conventional superconductors.

Recently, we proposed an alternative experimental approach to generate dendritic avalanches in YBCO films [27,28]. Unlike previous experiments in which the instability was triggered by the external magnetic field, in our work the instability was triggered by high magnetic field ramp rate, $\dot{B}_a$, (up to 3 kT/s), exploiting a unique, recently built, ultrafast MO system [29]. In the present work we trace the crossover of the flux penetration process into YBCO films from smooth, gradual penetration to dendritic avalanches, by changing both temperature and field ramp rate. Moreover, we experimentally determine the borderline in the $\dot{B}_a$-T plane separating regions of these two types of flux penetration modes. Our study allows examination of theories relevant to the dendritic instability, focusing on the HTS properties.

In several theoretical works, efforts were made to explain the dendritic flux instability [30–35]. The flux behavior was examined by solving the coupled differential equations for flux diffusion and thermal diffusion, for either a slab [31] or a thin superconducting film, taking into account nonlocal electrodynamics and heat exchange with the substrate [32–35]. In these theories, the rate of change of the external field, $\dot{B}_a$, plays a role in generating flux instabilities. Our experimental results show an increase of the threshold ramp rate, $\dot{B}_{th}$, with temperature, consistent with the predictions of Aranson *et al.* [35]. Based on the above theories we also propose an explanation as to why the HTSs are more stable than many conventional superconductors, requiring an extremely fast ramp rate to generate the dendritic instability, as in our YBCO films. Finally, we compare and discuss the morphology of the dendritic flux structures as it changes with the field ramp rate and temperature.

II. EXPERIMENT

YBCO films with a thickness of 150 nm were produced by thermal reactive coevaporation [36] on substrates made of yttrium stabilized zirconia (YSZ). This choice of substrate material is due to its relatively low thermal conductivity, which facilitates dendritic formation [28]. The films were epitaxially grown, with the c axis perpendicular to the surface. The samples were cut into $4\times4\,mm^2$ plates, suitable for magnetization measurements in a 5-T Quantum Design MPMS magnetometer and MO imaging in our custom-made system [29]. The MO apparatus enables real time imaging at rates up to 70 000 frames per second allowing exploration of flux dynamics in the superconducting films down to a time scale of 15 μs. The system provides a maximum applied field of 60 mT, which can be ramped at rates up to 3 kT/s.

The films were characterized magnetically, measuring their magnetization as a function of temperature and field, using the MPMS magnetometer. The inset to Fig. 1(a) shows the zero-field-cooled (lower line) and field-cooled (upper line) magnetization versus temperature, measured with an applied

 ©2016 American Physical Society

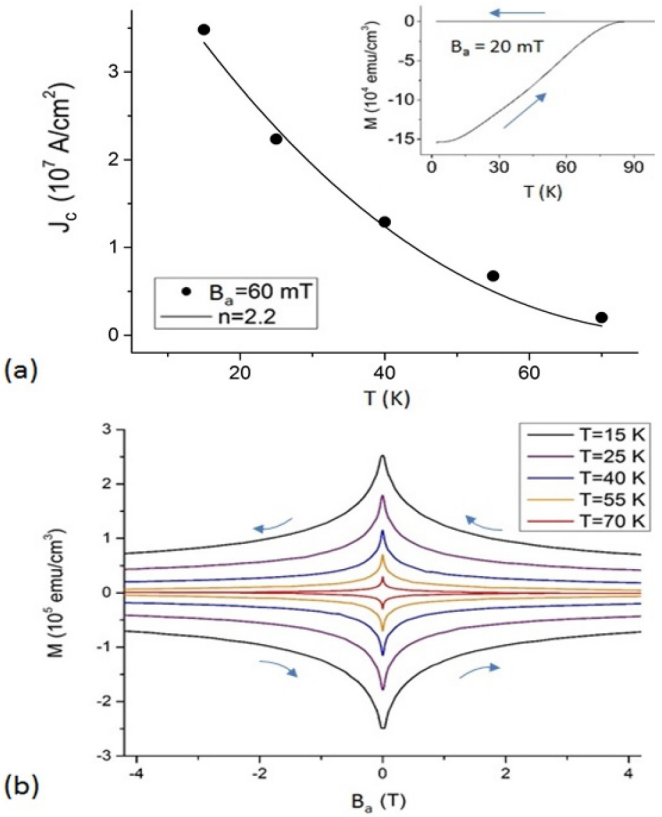

FIG. 1. (a) The temperature dependence of J_c for $B_a = 60$ mT, estimated from the magnetization curves of (b). The solid line through the J_c data points is a fit to $J_c \propto (1 - T/T_c)^n$, with $n = 2.2$. The inset to (a) shows the temperature dependence of the zero-field-cooled (lower line) and field-cooled (upper line) magnetization versus temperature, measured with an applied field $B_a = 20$ mT.

field $B_a = 20$ mT. The two curves demonstrate that superconductivity in this sample vanishes at $T_c \sim 85$ K. Figure 1(b) shows the magnetization-versus-field loops between -5 T and 5 T for temperatures between 15 and 70 K. Note that all the hysteresis loops have peaks at $B_a = 0$, confirming [37] the excellent uniformity of the sample. We further characterized the films by evaluating the critical current, J_c, from the measured M-B_a loops, using the Bean model formula [38,39]:

$$J_c = \frac{30\Delta M}{w}, \tag{1}$$

where ΔM is the width of the magnetization loop measured in emu/cm^3, and w is the lateral dimension of the square film (4 mm in our case). Figure 1(a) presents the resulting J_c values as a function of temperature for field $B_a = 60$ mT, corresponding to maximum external field used in the MO measurements. The solid line in the figure is a fit of the experimental $J_c(T)$ to a power law: $J_c \sim (1–T/T_c)^n$ with exponent $n \approx 2.2$. Similar results for the temperature dependence of J_c in thin YBCO films were reported in, e.g., Refs. [40,41].

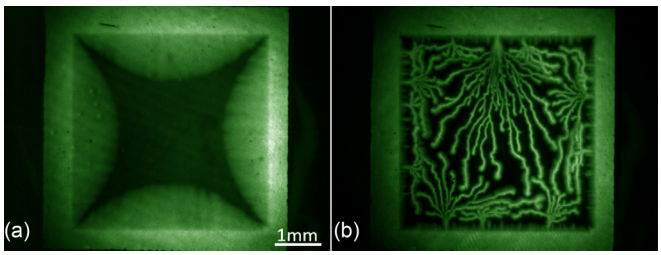

FIG. 2. Magneto-optical images of a zero-field-cooled YBCO film at $T = 7$ K, after exposing it to a perpendicular magnetic field $B_a = 60$ mT. The field was ramped up (a) at a conventional, slow ramp rate, ~ 1 mT/s, producing a Bean-like flux penetration, and (b) at an ultrafast ramp rate of 3 kT/s, generating dendritic flux penetration.

III. MAGNETO-OPTICAL RESULTS

The dramatic influence of the rate of change of the external field on the magnetic flux penetration into the YBCO films is demonstrated in Fig. 2. Figure 2(a) shows a MO image of one of the YBCO films, taken after it was zero-field cooled (ZFC) to 7 K and then exposed to a perpendicular external field ramped from zero to $B_a = 60$ mT at a rate of $\sim$1 mT/s. The resulting flux penetration is smooth, with a Bean-like distribution.

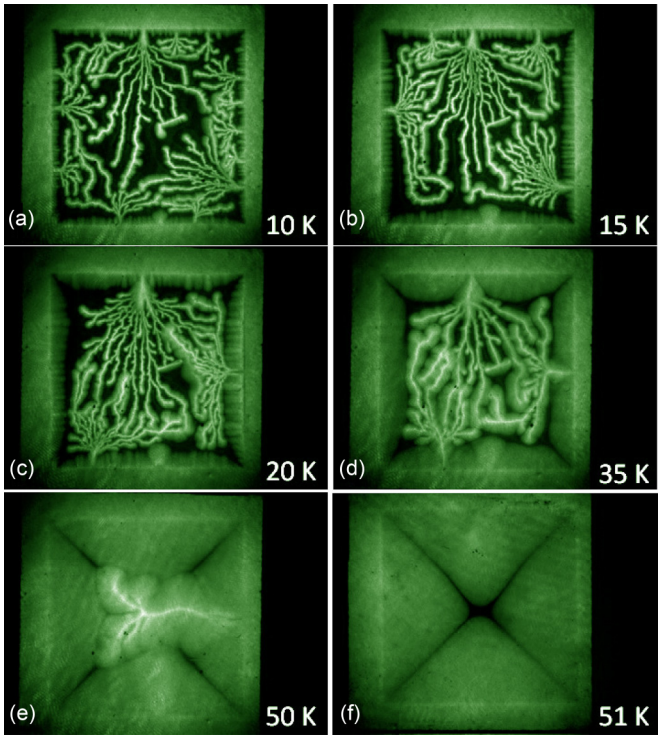

FIG. 3. (a–f) Magneto-optical images of the YBCO film, after ramping the applied field from zero to 60 mT at 3 kT/s, measured at $T = 10$, 15, 20, 35, 50, and 51 K, respectively. The sample was heated and zero-field cooled between each experiment. The number of separate dendrites decreases while the film temperature is increased. The number of branches in each dendrite was the highest at the intermediate temperature of $T = 20$ K. $T = 51$ K is the threshold temperature for this sample; no instability appeared above this temperature.

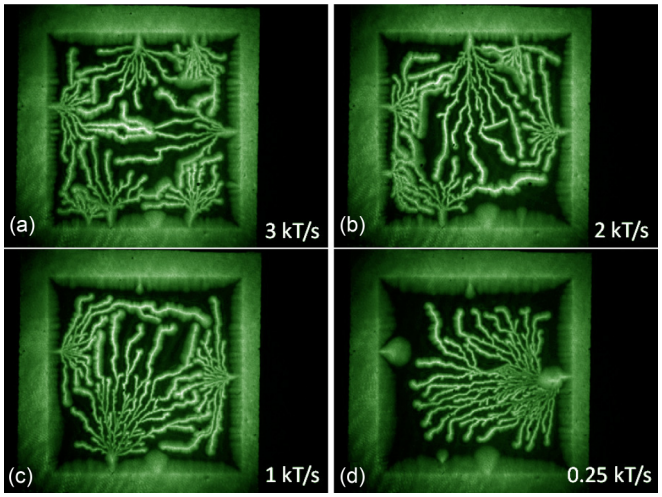

FIG. 4. (a–d) Magneto-optical images of the YBCO film measured at 15 K, exposed to a field ramp from zero to 60 mT, at rates of 3, 2, 1, and 0.25 kT/s. The number of dendrites reduces with decreasing ramp rates while the number of branches, and the size of each individual dendrite, grows larger.

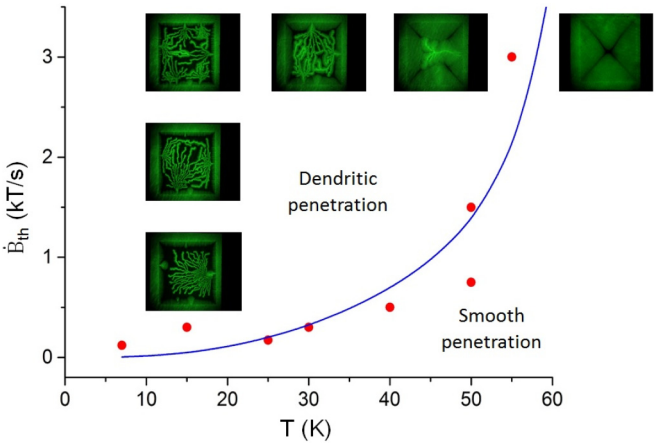

FIG. 5. "Stability diagram" showing the dendritic and smooth penetration regions in a $\dot{B}_{th}$-T plane. The circles are the experimental data; each point represents the minimum ramp rate required to trigger the instability at a specific temperature. The solid line shows the temperature dependence of $\dot{B}_{th}$ predicted by Eq. (5). The insets are images taken from Figs. 2–4, showing evolution of the dendritic morphology as the crossover line is approached.

Repeating the same experiment as described above, but with a 3 kT/s sweep rate of the applied field, produced extremely different flux structures, namely, the dendritic flux instability shown in Fig. 2(b).

Figures 3 and 4 display the effect of temperatures and sweep rates, respectively, on the dendritic flux structure. The images in Fig. 3 were taken after zero-field-cooling the film to the indicated temperatures and then ramping the field from 0 to 60 mT at a rate of 3 kT/s. The images show a crossover from dendritic avalanches at low and moderate temperatures to a Bean-like penetration [42] at a threshold temperature $T_{th} =$ 50 K. Repeating the same experiment at slower ramp rates results in a lower threshold temperature, for example, $T_{th} = 40$ and 15 K for sweep rates of 0.5 and 0.2 kT/s, respectively.

As apparent from the images of Fig. 3, the morphology of the dendritic avalanches is also temperature dependent. Specifically, at 7 K [Fig. 3(a)] the dendritic penetration nucleates at several locations ("trunks") at the film edges. Upon increasing temperature, the number of trunks decreases, while the number of branches in each dendritic structure initially increases (up to $T \sim 25$ K) and then decreases. Also note that the images at the highest temperatures (40–50 K) exhibit "diffused," thicker branches.

A change in the character of the field penetration from dendritic avalanches to a Bean profile can also be obtained by changing the field ramp rate at a constant temperature. This is demonstrated in Fig. 4 which shows MO images recorded at 15 K, after the field was increased from zero to 60 mT with ramp rates ranging from 0.25 to 3 kT/s. Between the different ramp rate experiments the sample was heated above T_c and then again cooled in zero field. Figure 4(a), taken after the fastest ramping (3 kT/s), shows multiple separate dendritic avalanches each with relatively few branches. As the field ramp rates decrease [Figs. 4(b)–4(d)], the number of separate avalanche events decreases but each event develops an increasing number of branches. As the rate drops below 0.2 kT/s, the dendrites disappear altogether and a Bean profile is established as shown in Fig. 2(a). Note the appearance of a defect in the left side of the film in Fig. 4(d). This defect is absent in Fig. 2(a), recorded before the experiments generating avalanches had started. As discussed in Ref. [27], the aggressive avalanche events frequently cause permanent damage in YBCO films due to the excess heat release.

Crossover between dendritic and smooth flux penetration were observed in a set of field ramp rates and temperatures as summarized in Fig. 5 in a $\dot{B}_{th}$ versus T diagram. The circles in the figure are the experimental data; each represents the minimum ramp rate required to trigger the instability at a specific temperature. The calculated solid line, to be discussed in the next section, increases monotonically with temperature, describing well the experimental data. This line separates the quasiequilibrium region, where the smooth penetrating front follows the Bean model, from the nonequilibrium region where dendrites are observed. Figure 5 incorporates several of the images of Figs. 3 and 4 to demonstrate evolution of dendritic structures as the crossover line is approached either by changing temperature or field ramp rate.

IV. DISCUSSION

The data show that a crossover between these two modes can be achieved, e.g., by changing the field ramp rate at a constant temperature (Fig. 4), or by changing temperature at a constant field ramp rate (Fig. 3). As this line is approached, the dendrites' morphology changes, namely, the number of dendritic nucleation points decreases and, concurrently, the number of branches tends to increase. In the following we discuss the behavior of the crossover line as well as the dendrite morphology.

The monotonic increase of $\dot{B}_{th}(T)$ with temperature can be intuitively understood as follows. The triggering of a dendrite depends on flux motion and the associated local increase in

temperature [21], making the resistance of the superconducting film to the penetration of magnetic flux very important. Edge defects can facilitate flux entry and flux motion, and enhance local heating [43]. Clearly, at higher temperatures, as the system globally becomes more susceptible to flux entry, this local mechanism is weakened and the buildup of heat is reduced. Consequently, a more aggressive, faster application of the external field is required to create the conditions for the thermomagnetic breakdown. The critical current density, $J_c(T)$, may serve as a measure for the resistance of the system to flux entry. Thus, at low temperatures, where flux pinning is relatively strong (J_c is large) and flux entry is difficult, the condition for a breakdown is achieved at relatively low field ramp rates. At high temperatures (J_c is small) the sample allows easy entry of vortices even at moderate field ramp rates and magnetic avalanches will be achieved only at ultrahigh rates. Clearly, the temperature dependence of the thermal parameters, such as the heat transfer between the superconducting film and the substrate should also be taken into account. As this parameter is expected to increase with temperature [44,45], heat transfer from the film to the substrate is enhanced, requiring higher field ramp rates for dendritic formation. This intuitive explanation is consistent with the theoretical predictions of Aranson *et al.* [35], where a coupling of the nonlocal magnetic flux diffusion with the local thermal diffusion leads to a prediction of the threshold field ramp rate, $\dot{B}_{th}$, above which dendrites should appear. These authors describe the spatial and temporal distribution of the magnetic induction $\boldsymbol{B}(\boldsymbol{r},t)$ and temperature $T(\boldsymbol{r},t)$ by the Maxwell equations coupled to heat diffusion:

$$C\frac{\partial T}{\partial t} = \nabla\kappa\nabla T - (T - T_0)h/d + \boldsymbol{J}E, \tag{2}$$

$$\frac{\partial \boldsymbol{B}}{\partial t} = -\nabla x\boldsymbol{E}, \quad \nabla x\boldsymbol{H} = \boldsymbol{J}\delta(z), \tag{3}$$

where C, κ, h, d, $\boldsymbol{E}$, and $\boldsymbol{J}$ are the heat capacity, thermal conductivity, heat transfer coefficient to the substrate held at the temperature T_0, the sample thickness, the electric field, and the sheet current, respectively. The three terms on the right-hand side of Eq. (2) describe the thermal diffusion, the heat relaxation, and the Joule heating, respectively. Importantly, this Joule term couples the two equations.

The flux stability is controlled by the parameter $\tau_0 = D_h/D_m$, the ratio of magnetic and thermal diffusion coefficients, expressed as $D_h = \kappa/C$ and $D_m = \rho_F/\mu_0$. Here the flux flow resistivity $\rho_F = \rho_n B_a/B_{c2}$ and μ_0 is the magnetic permeability. In addition, due to nonlocality, in thin films the τ parameter will be modified according to $\tau = \tau_0 d/2L_h$, where L_h, the thermal length, is defined as $L_h = (d\kappa/h)^{1/2}$. Combining the previous relations one obtains [35]

$$\tau = \frac{\mu_0\sqrt{d\kappa h}}{2\rho_F C}. \tag{4}$$

For $\tau \ll 1$, i.e., the heat diffusion is much slower than the magnetic diffusion; dendritic flux structures are favored. In this case, the theory predicts that the threshold ramp rate of the applied field, $\dot{B}_{th}$, is given by

$$\dot{B}_{th} \sim \frac{h/b}{J_c(T)|\partial J_c(T)/\partial T|}, \tag{5}$$

where $b = [1 - 1/\cosh(B_a/B_p)]w/2$ is the width of the flux-penetrated critical state region, w is the film width, B_a is the external field, and $B_p = \mu_0 J_c d/\pi$, where d is the thickness of the film [46]. The solid line in Fig. 5 was calculated using Eq. (5), taking the experimental temperature dependence of $J_c \sim (1–T/T_c)^{2.2}$ and assuming that $h \sim T^3$ [44,45]. Apparently, the calculated line agrees qualitatively well with the experimental data. A quantitative analysis could not be pursued because of the lack of information on several of the material and substrate parameters, in particular the heat conductivity to the substrate, and its temperature dependence at cryogenic temperatures.

While high ramp rates ($\dot{B}_{th}$ of order kT/s) were required to generate dendritic flux patterns in our YBCO films, the ramp rates in conventional superconductors are practically zero in comparison. In fact, the "stability diagram" in conventional superconductors was determined by a threshold field, B_{th}, rather than threshold ramp rate $\dot{B}_{th}$ [18]. An explanation to the relative stability of HTS to dendritic avalanches at low ramp rates can be based on Eq. (4). The parameter τ in this equation depends on the flux flow resistance, ρ_F, and several thermal parameters (κ, C, h). We argue that the difference in the thermal parameters in HTS and conventional superconductors cannot explain the dramatic difference in the stability of these materials to flux avalanches. The parameter h cannot be a crucial factor as both YBCO and MgB_2 are dendritic when various substrate materials are used. The ratio κ/C is intimately related to the thermal diffusion of the films. Comparing, for example, YBCO with MgB_2 reveals that this ratio is significantly lower in magnitude for the HTS material. (At $T/T_c \sim 0.1$, which is in the "dendritic phase" for both MgB_2 and YBCO, the κ value is about two times larger in YBCO, while C is more than an order of magnitude higher [47–50]). Hence, a consideration of only the thermal parameters in the expression for τ [Eq. (4)] leads to a lower value of τ for the HTS materials, implying that HTS should be less stable than the conventional superconductors. Thus, the thermal parameters fail to explain the stability of HTS films. We therefore assert that the key parameter in the equation is the flux flow resistivity, $\rho_F = \rho_n B_a/B_{c2}$. From Eq. (4) it is clear that for a material to be stable ρ_F should be low. This can be achieved by either having a smaller value of ρ_n or larger B_{c2}. Since the normal state resistivity, ρ_n, is larger in HTS than in conventional superconductors, it cannot explain the stability of these materials. The critical field B_{c2}, however, is larger by orders of magnitude in HTS when compared to the conventional materials, yielding a lower value of ρ_F. This result implies a higher stability against flux avalanches in HTS films, a stability that can be overcome by applying high electric field [21] or, equivalently, by a rapid change of the external magnetic field as done in our experiment.

Our assertion that ρ_F is the main factor in determining the stability of the superconductor against flux avalanches finds support in recent MO studies, comparing MgB_2 films with different ρ_F [51,52]. In these studies dendrites were easily

triggered by a 100-mT field in films with $\rho_F \approx 0.16\,\mu\Omega\,\mathrm{cm}$, but have never been observed in ultrapure films with $\rho_F \approx 0.006\,\mu\Omega\,\mathrm{cm}$, demonstrating that ρ_F is a key parameter in the stability of the film against dendritic avalanches. By passing, we note that our attempts to generate dendrites in the ultrapure MgB_2 using field ramp rates up to 3 kT/s were unsuccessful. This can be understood noticing that ρ_F for ultrapure MgB_2 is significantly lower than $\rho_F = 0.05\,\mu\Omega\,\mathrm{cm}$ in our YBCO, taking $B_a = 100\,\mathrm{mT}$, $B_{c2} = 120\,\mathrm{T}$, and $\rho_n \approx 60\,\mu\Omega\,\mathrm{cm}$ [53].

The data of Figs. 3–5 show that the morphology of the dendrites in the unstable regions changes as the crossover line to a smooth penetration is approached, either by changing temperature or field ramp rate. Basically, the number of dendritic trunks decreases while the number of branches tends initially to increase. The dendritic flux morphology was also the focus of previous works on conventional superconductors, where dendrites were generated by changing B_a quasistatically [11,18,33]. It has been reported that the morphology of the dendritic structures is strongly temperature dependent with a tendency similar to that reported here for YBCO films. Namely, at low temperatures the dendrites were numerous with few branches, while at temperatures just below the threshold only large treelike structures were seen. However, no ramp rate dependence was reported in the previous studies.

Following our qualitative explanation of the crossover line, the observed morphology variations as the line is approached can also be understood considering changes in the resistance of the superconducting film to the penetration of magnetic flux as T and $\dot{B}_a$ vary. As the temperature increases at a constant $\dot{B}_a$, the system becomes "softer," i.e., more susceptible to smooth flux entry, and the probability for dendritic flux penetration decreases. Consequently, the number of dendritic trunks decreases. Also, the dendritic breakdowns occur at higher external field, B_a, allowing for a more developed dendrite with more branches. At even higher temperatures, the development of the dendrite is reversed, displaying fewer branches. Two mechanisms might contribute to this. First, the gradual change in thermal parameters increases the heat diffusion considerably, decreasing the efficiency of the avalanche and reducing the number of branches. The second mechanism is an increased flux relaxation, which significantly widened the branches. A similar situation occurs when the ramp rate is changed. As the probability for dendritic avalanche decreases upon decreasing $\dot{B}_a$, at slower ramp rate dendritic avalanches will be produced at higher fields creating fewer dendrites with more flux, i.e., with more branches. Fast ramping on the other hand, will trigger more dendrites at lower fields and, therefore, less flux will be channeled into each.

V. SUMMARY AND CONCLUSIONS

Previous studies in conventional superconductors have shown that dendritic avalanches are triggered by applying magnetic field above a certain threshold. Our measurements in YBCO films show that the rate of change of the external field also plays an important role. By varying the field ramp rate at different temperatures, we are able to experimentally determine the borderline in the $\dot{B}_a$-T plane separating regions of smooth and dendritic flux penetration. This line increases monotonically with temperature, consistent with the predictions of Aranson *et al.* [35]. Within the dendritic instability region, the morphology of the dendrites changes as the borderline is approached, either by changing the temperature or the ramp rate. An intuitive explanation to the behavior of the borderline, as well as the dendritic morphology, has been given in terms of the susceptibility of the system to flux entry, which depends on B_a and T. The present work has demonstrated the dependence of the complex dendritic phenomena on temperature and rate of change of the external magnetic field. Clearly, the phenomena also depend on the magnetic field itself. A further work is needed to establishing the stability in three dimensions (3D), namely, field, rate of change of field, and temperature. Different 3D diagrams are expected for superconducting materials with different flux flow resistivity, ρ_F, which we have identified as a dominant parameter influencing the stability of a superconducting film. For materials with a relatively small ρ_F, such as YBCO, large B_a are required to generate the instability, whereas for materials with large ρ_F, such as MgB_2, dendrites can be generated by quasistatic changes in B_a.

ACKNOWLEDGMENTS

The authors thank Dr. Robert Semerad for preparing samples and helpful discussions. Important discussions with Professor Emeritus Yuri Galperin and Associate Professor Jørn Inge Vestgården are acknowledged. We also acknowledge financial support from the Israel Science Foundation (Grant No. ISF-164/12) and the Norwegian Research Council.

[1] V. Vlasko-Vlasov, V. Nikitenko, A. Polyanskii, G. Crabtree, U. Welp, and B. Veal, Phys. C (Amsterdam, Neth.) **222**, 361 (1994).
[2] M. Koblischka, T. Johansen, M. Baziljevich, H. Hauglin, H. Bratsberg, and B. Y. Shapiro, Europhys. Lett. **41**, 419 (1998).
[3] R. Surdeanu, R. J. Wijngaarden, E. Visser, J. M. Huijbregtse, J. H. Rector, B. Dam, and R. Griessen, Phys. Rev. Lett. **83**, 2054 (1999).
[4] D. Barness, M. Sinvani, A. Shaulov, T. Tamegai, and Y. Yeshurun, Phys. Rev. B **77**, 094514 (2008).
[5] S. Field, J. Witt, F. Nori, and X. Ling, Phys. Rev. Lett. **74**, 1206 (1995).
[6] E. R. Nowak, O. W. Taylor, L. Liu, H. M. Jaeger, and T. I. Selinder, Phys. Rev. B **55**, 11702 (1997).
[7] E. Altshuler and T. Johansen, Rev. Mod. Phys. **76**, 471 (2004).
[8] M. Wertheimer and J. le G. Gilchrist, J. Phys. Chem. Solids **28**, 2509 (1967).
[9] C. A. Duran, P. L. Gammel, R. E. Miller, and D. J. Bishop, Phys. Rev. B **52**, 75 (1995).

[10] E. Altshuler, T. H. Johansen, Y. Paltiel, P. Jin, K. E. Bassler, O. Ramos, Q. Y. Chen, G. F. Reiter, E. Zeldov, and C. W. Chu, Phys. Rev. B **70**, 140505(R) (2004).
[11] I. A. Rudnev, D. V. Shantsev, T. H. Johansen, and A. E. Primenko, Appl. Phys. Lett. **87**, 042502 (2005).
[12] V. V. Yurchenko, D. V. Shantsev, T. H. Johansen, M. R. Nevala, I. J. Maasilta, K. Senapati, and R. C. Budhani, Phys. Rev. B **76**, 092504 (2007).
[13] P. Mikheenko, T. H. Johansen, S. Chaudhuri, I. J. Maasilta, and Y. M. Galperin, Phys. Rev. B **91**, 060507(R) (2015).
[14] I. Rudnev, S. Antonenko, D. Shantsev, T. Johansen, and A. Primenko, Cryogenics **43**, 663 (2003).
[15] V. Vlasko-Vlasov, U. Welp, V. Metlushko, and G. Crabtree, Phys. C (Amsterdam, Neth.) **341-348**, 1281 (2000).
[16] F. Colauto, M. Motta, A. Palau, M. Blamire, T. Johansen, and W. Ortiz, IEEE Trans. Appl. Supercond. **25**, 1 (2015).
[17] M. Baziljevich, A. Bobyl, D. Shantsev, E. Altshuler, T. Johansen, and S. Lee, Phys. C (Amsterdam, Neth.) **369**, 93 (2002).
[18] T. Johansen, M. Baziljevich, D. Shantsev, P. Goa, W. Kang, H. Kim, E. Choi, M.-S. Kim, and S. Lee, Europhys. Lett. **59**, 599 (2002).
[19] A. Bobyl, D. Shantsev, T. Johansen, W. Kang, H. Kim, E. Choi, and S. Lee, Appl. Phys. Lett. **80**, 4588 (2002).
[20] F. L. Barkov, D. V. Shantsev, T. H. Johansen, P. E. Goa, W. N. Kang, H. J. Kim, E. M. Choi, and S. I. Lee, Phys. Rev. B **67**, 064513 (2003).
[21] J. Albrecht, A. Matveev, M. Djupmyr, G. Schütz, B. Stuhlhofer, and H.-U. Habermeier, Appl. Phys. Lett. **87**, 182501 (2005).
[22] Åge Andreas Falnes Olsen, T. H. Johansen, D. Shantsev, E.-M. Choi, H.-S. Lee, H. J. Kim, and S.-I. Lee, Phys. Rev. B **74**, 064506 (2006).
[23] S. Treiber, C. Stahl, G. Schütz, and J. Albrecht, Phys. Rev. B **84**, 094533 (2011).
[24] V. Bujok, P. Brüll, J. Boneberg, S. Herminghaus, and P. Leiderer, Appl. Phys. Lett. **63**, 412 (1993).
[25] P. Leiderer, J. Boneberg, P. Brüll, V. Bujok, and S. Herminghaus, Phys. Rev. Lett. **71**, 2646 (1993).
[26] U. Bolz, B. Biehler, D. Schmidt, B.-U. Runge, and P. Leiderer, Europhys. Lett. **64**, 517 (2003).
[27] M. Baziljevich, E. Baruch-El, T. Johansen, and Y. Yeshurun, Appl. Phys. Lett. **105**, 012602 (2014).
[28] E. Baruch-El, M. Baziljevich, T. Johansen, and Y. Yeshurun, J. Supercond. Novel Magn. **28**, 379 (2015).
[29] M. Baziljevich, D. Barness, M. Sinvani, E. Perel, A. Shaulov, and Y. Yeshurun, Rev. Sci. Instrum. **83**, 083707 (2012).
[30] R. Mints and A. Rakhmanov, Rev. Mod. Phys. **53**, 551 (1981).
[31] E. E. Dvash, I. Shapiro, and B. Ya. Shapiro, Phys. Rev. B **80**, 134522 (2009).
[32] D. V. Denisov, A. L. Rakhmanov, D. V. Shantsev, Y. M. Galperin, and T. H. Johansen, Phys. Rev. B **73**, 014512 (2006).
[33] J. I. Vestgården, D. V. Shantsev, Y. M. Galperin, and T. H. Johansen, Phys. Rev. B **84**, 054537 (2011).
[34] J. Vestgården, D. Shantsev, Y. Galperin, and T. Johansen, Supercond. Sci. Technol. **26**, 055012 (2013).
[35] I. S. Aranson, A. Gurevich, M. S. Welling, R. J. Wijngaarden, V. K. Vlasko-Vlasov, V. M. Vinokur, and U. Welp, Phys. Rev. Lett. **94**, 037002 (2005).
[36] B. Utz, R. Semerad, M. Bauer, W. Prusseit, P. Berberich, and H. Kinder, IEEE Trans. Appl. Supercond. **7**, 1272 (1997).
[37] D. V. Shantsev, M. R. Koblischka, Y. M. Galperin, T. H. Johansen, L. Půst, and M. Jirsa, Phys. Rev. Lett. **82**, 2947 (1999).
[38] E. Gyorgy, R. Van Dover, K. Jackson, L. Schneemeyer, and J. Waszczak, Appl. Phys. Lett. **55**, 283 (1989).
[39] H. Wiesinger, F. M. Sauerzopf, and H. W. Weber, Phys. C (Amsterdam, Neth.) **203**, 121 (1992).
[40] W. Xing, B. Heinrich, J. Chrzanowski, J. Irwin, H. Zhou, A. Cragg, and A. Fife, Phys. C (Amsterdam, Neth.) **205**, 311 (1993).
[41] M. Ohmukai, T. Fujita, and T. Ohno, Braz. J. Phys. **31**, 511 (2001).
[42] T. Schuster, H. Kuhn, E. H. Brandt, M. V. Indenbom, M. Kläser, G. Müller-Vogt, H. U. Habermeier, H. Kronmüller, and A. Forkl, Phys. Rev. B **52**, 10375 (1995).
[43] D. V. Denisov, D. V. Shantsev, Y. M. Galperin, E.-M. Choi, H.-S. Lee, S.-I. Lee, A. V. Bobyl, P. E. Goa, A. A. F. Olsen, and T. H. Johansen, Phys. Rev. Lett. **97**, 077002 (2006).
[44] E. T. Swartz and R. O. Pohl, Rev. Mod. Phys. **61**, 605 (1989).
[45] S. Pu, thesis, Department of Physics, McGill University Montréal, Québec, Canada, 1999.
[46] E. Zeldov, J. R. Clem, M. McElfresh, and M. Darwin, Phys. Rev. B **49**, 9802 (1994).
[47] M. Schneider, D. Lipp, A. Gladun, P. Zahn, A. Handstein, G. Fuchs, S.-L. Drechsler, M. Richter, K.-H. Müller, and H. Rosner, Phys. C (Amsterdam, Neth.) **363**, 6 (2001).
[48] B. Terzijska, R. Wawryk, D. Dimitrov, C. Marucha, V. Kovachev, and J. Rafalowicz, Cryogenics **32**, 53 (1992).
[49] H. D. Yang, J.-Y. Lin, H. H. Li, F. H. Hsu, C.-J. Liu, S.-C. Li, R.-C. Yu, and C.-Q. Jin, Phys. Rev. Lett. **87**, 167003 (2001).
[50] K. A. Moler, D. J. Baar, J. S. Urbach, R. Liang, W. N. Hardy, and A. Kapitulnik, Phys. Rev. Lett. **73**, 2744 (1994).
[51] Z. Ye, Q. Li, Y. Hu, A. Pogrebnyakov, Y. Cui, X. Xi, J. Redwing, and Q. Li, IEEE Trans. Appl. Supercond. **15**, 3273 (2005).
[52] Z. Ye, Q. Li, Y. Hu, A. Pogrebnyakov, Y. Cui, X. Xi, J. Redwing, and Q. Li, Appl. Phys. Lett. **85**, 5284 (2004).
[53] M. Cyrot and D. Pavuna, *Introduction to Superconductivity and High- Materials* (World Scientific, Singapore, 1992).